

www.acsami.org Research Article

# One-Step Synthesis and Operando Electrochemical Impedance Spectroscopic Characterization of Heterostructured MoP-Mo<sub>2</sub>N Electrocatalysts for Stable Hydrogen Evolution Reaction

Navid Attarzadeh, Ambadi Lakshmi-Narayana, Debabrata Das, Susheng Tan, Vaithiyalingam Shutthanandan, and C.V. Ramana\*



**Cite This:** ACS Appl. Mater. Interfaces 2024, 16, 6958–6970



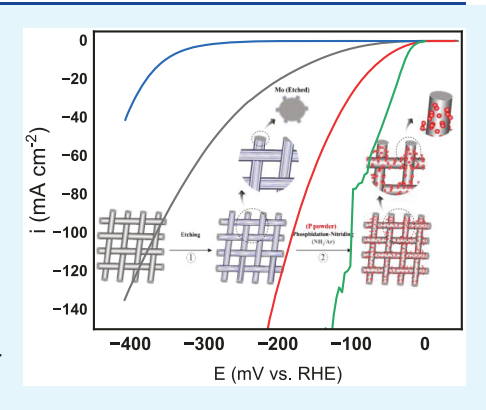
**ACCESS** 

III Metrics & More

Article Recommendations

Supporting Information

ABSTRACT: This study presents a novel synthesis of self-standing MoP and Mo<sub>2</sub>N heterostructured electrocatalysts with enhanced stability and catalytic performance. Facilitated by the controlled phase and interfacial microstructure, the seamless structures of these catalysts minimize internal resistivity and prevent local corrosion, contributing to increased stability. The chemical synthesis proceeds with an etching step to activate the surface, followed by phosphor-nitriding in a chemical vapor deposition chamber to produce MoP–Mo<sub>2</sub>N@Mo heterostructured electrocatalysts. X-ray diffraction analyses confirmed the presence of MoP, Mo<sub>2</sub>N, and Mo phases in the electrocatalyst. Morphology studies using scanning electron microscopy characterize the hierarchical growth of structures, indicating successful formation of the heterostructure. X-ray photoelectron spectroscopy (XPS) analyses of the assynthesized and postcatalytic activity samples reveal the chemical shift in terms of the binding energy (BE) of the Mo 3d XPS peak, especially after catalytic activity. The



XPS BE shifts are attributed to changes in the oxidation state, electron transfer, and surface reconstruction during catalysis. Electrochemical evaluation of the catalysts indicates the superior performance of the MoP-Mo<sub>2</sub>N@Mo heterostructured catalyst in hydrogen evolution reactions (HER), with lower overpotentials and enhanced Tafel slopes. The stability tests reveal changes in double layer capacitance over time, suggesting surface reconstruction and an increased active surface area during catalysis. Operando electrochemical impedance spectroscopy (EIS) further elucidates the dynamic changes in resistance and charge transfer during HER. Overall, a comprehensive understanding of the synthesis, characterization, and electrochemical behavior of the developed MoP-Mo<sub>2</sub>N@Mo heterostructured electrocatalyst, as presented in this work, highlights its potential utilization in sustainable energy applications.

KEYWORDS: Electrocatalysts, Hydrogen Evolution Reaction, Molybdenum Phosphide, Molybdenum Nitride, Stability, Operando-EIS

# **■ INTRODUCTION**

Hydrogen, as a clean alternative source, is in stark contrast to fossil fuels, a leading cause of global warming and climate change. Hydrogen promotes zero carbon emissions during use, reduces harmful substances' release, and provides a potential for carbon-neutral energy production. Hydrogen generated from renewables may also be crucial in the future for refueling transportation infrastructure in addition to balancing out erratic output. However, there are a number of scientific challenges associated with hydrogen that must be overcome for it to become a sustainable and widespread energy source.<sup>2,3</sup> The progress and expansion of "green" hydrogen production using the electrolysis method depend on developing durable electrocatalysts tolerating high current densities for a prolonged time. In addition, hydrogen evolution reaction (HER) is limited by a significant overpotential.<sup>4-6</sup> Platinum group metals (PGM) demonstrated relatively low overpotentials for HER across a wide pH range of electrolytes. 7-10

However, the large-scale utilization of Pt electrocatalysts is hindered by their scarcity and the associated high cost, limiting their widespread applications. Significant research efforts are focused on developing alternatives to reduce the reliance on PGM catalysts. These efforts are aimed at synthesizing efficient and affordable catalysts using abundant and low-cost elements and optimizing their structures while maintaining high catalytic activity and stability for hydrogen production. Although The durability and longevity of electrocatalysts are essential because the degradation of catalysts over time decreases efficient operation and leads to higher energy

Received: September 25, 2023 Revised: January 11, 2024 Accepted: January 15, 2024 Published: February 2, 2024





costs, 4,11,18 During HER, the catalysts are subjected to harsh electrochemical conditions, leading to various degradation mechanisms that can negatively impact the catalyst's stability and performance over time. The contributions of several factors determine the stability of electrocatalysts. The chemical, electrochemical, and morphological stabilities of catalysts in the electrolyte environment are essential. The catalyst should resist dissolution, particle detachment, and reactions leading to the loss of active sites and withstand the high applied current densities over a broad pH range without significant alteration of its catalytic activity. In addition, poisoning or deactivation by adsorbed impurities and reaction with intermediates reduces the catalytic activity. Therefore, the scientific and engineering research community is actively exploring various synthesis strategies with different materials to enhance the stability of electrocatalysts for the HER.

Of the particular PGM-free catalysts, Mo-based compounds, such as  ${\rm MoS_2}^{12}~{\rm S_{doped}}$ - ${\rm MoO_w}^{13}~{\rm MoN_w}^{14}~{\rm Mo_3B}$ , and  ${\rm MoP}$ , such as  ${\rm MoS_2}^{12}$  or  ${\rm MoP}$ , such as  ${\rm MoS_2}^{12}$  or  ${\rm MoP}$ , such as  ${\rm MoS_2}^{12}$  or  ${\rm MoS_2}^{12}$  or  ${\rm MoS_2}^{13}$  or  ${\rm MoS_2}^{13}$ could possess promising longevity with their efficient HER catalytic activities because they contain Pt-like d-band electronic configuration. In fact, as presented and discussed in a recent review and references therein, 20 Mo-based compounds (oxides, sulfides and nitrides) proved to be quite useful for many industrial applications, particularly in the emerging fields of energy and electronics. 12-16,20-24 Herein, we are interested in taking advantage of chemically distinct heterostructured catalysts, where engineering the Mophosphide (Mo-P) system with another chemical compound of Mo integrated. Generally, P atoms with higher electronegativity draw electrons from transition metals and function as a Lewis-base to attract positively charged protons in the HER process.<sup>25</sup> Further enhancement in the HER catalytic activity could be achieved through S doping into the MoP structure, where the synergistic effects between S and P created a more active electrode.26 Introducing a second anion generates heterostructured catalysts, where combined with nanostructured architecting, the electronic features and efficiency can be tuned significantly. 16 From the perspective of the HER catalytic activity, most heterostructured catalysts, either with active/active or active/nonactive structures, highlight various advantages as follows. First, the number of active sites increases significantly, and the electrical conductivity is enhanced because refining the nanostructure creates sufficient adsorption sites for the intermediates of HER.<sup>27</sup> Second, using macroscopic and seamless substrates such as mesh provides fast mass diffusion that can reduce overpotentials at high current densities. 16 Third, the electronegativity difference between different components of heterostructures accelerates the electron movements between components, which also results in electronic structure refinement. 28,29 Finally and most importantly, constructing heterostructures improves the catalysts' performance, durability, and longevity. Therefore, the paramount strategy of introducing nonmetals, such as N, P, and O, into ternary or quaternary heterostructures is tuning the chemical composition that can enhance the intrinsic catalytic activity, increase the number of active sites, and improve the longevity of efficient catalytic activity.

Recently, MoP-based heterojunction catalysts were developed for efficient HER performance. Yang et al. successfully synthesized the heterostructure catalyst of  $MoS_2-MoP$  anchored on the N-doped porous carbon (NC) substrate. The heterojunction catalyst exhibited significant catalytic

activity with remarkable stability for HER that could be derived from distinctive nanosheet morphology increasing active catalytic sites, the synergistic effect of MoP and MoS<sub>2</sub> phases, and efficient electron movements.31 Loomba et al. designed synthesizing porous nitrogen-doped NiMo<sub>3</sub>P (N-NiMo<sub>3</sub>P) microsheets.<sup>32</sup> They found that inducing nitrogen increased the corrosion resistance, and the higher electronegativity of nitrogen in metal-nitrogen bonds yielded greater stability of the active sites. In fact, the electron-withdrawing capability of nitrogen causes metal ions to achieve a higher valence state, which improves the electron transition and enhances mobilizing of the electronic density of the catalysts.<sup>32</sup> Gu et al. also synthesized a 2D porous MoP/Mo2N heterojunction by controllable pyrolysis of 2D PMo<sub>12</sub>-MA precursor.<sup>33</sup> The authors fabricated transition-metal interstitial compounds (TMICs) by pyrolyzing the complex of melamine (MA) and Keggin-structured [PMo<sub>12</sub>O<sub>40</sub>]<sup>3</sup>(PMo<sub>12</sub>), where the atomic nitrogen was obtained from the pyrolysis of MA units.<sup>33</sup> The HER performance could surpass the commercial Pt/c catalysts in a neutral medium.<sup>33</sup> Although significant development in various electrocatalysts was achieved for increasing efficiency and boosting performance, less attention has been devoted to an insightful understanding of inducing nonmetals on the durability of TMPs through electrochemical studies. 34,35 The fact that cannot be overlooked is the capability of active sites to undergo structural self-reconstruction during catalytic activity due to electrically driven structural reduction or oxidation processes.<sup>36</sup> In fact, the self-reconstruction could increase or decrease the catalytic activity.<sup>37</sup> The current ex-situ characterizations lack strong rationales for judiciously comprehending the rationale underlying the longevity of the catalyst's performance. However, operando or in situ techniques have attracted tremendous interest because of their ability to analyze real-time HER, capture dynamic evolutions in the structure and electronic features, and track the self-reconstruction of catalysts.<sup>38</sup> The latter feature is crucial in extending the durability of a catalyst because it particularly creates more active sites via the electrochemical activation process of the catalysts, which results in further boosting the catalytic activity. 38-40 With that being expressed, we aim to study the long-term stability and activity of the electrocatalysts developed via phosphidizing and nitriding of the molybdenum mesh. The source for N in the current study is NH<sub>3</sub> gas and all the new compounds formed on a sturdy Mo mesh, which is a seamless electrocatalyst. The electrocatalyst synthesized in Gu et al. study<sup>33</sup> needed to be applied on a conductive surface, such as graphite, which brought stability issues. In the current study, we synthesize a heterostructure of MoP-Mo<sub>2</sub>N on the Mo mesh surface and demonstrate prolonged stability. The novelty of the current study. regardless of the synthesize method, is to employ an operando-EIS technique along with the XPS study to record real-time electronic and compositional changes during electrocatalytic activity and correlating the significant durability to the ability of the composition to undergo a reconstruction process, where increasing the Mo<sup>2+</sup> concentration during electrocatalytic performance confirmed the objective. Based on our literature survey, no study has used Op-EIS so far for the HER performance that could suggest rationales about the surface reconstruction.

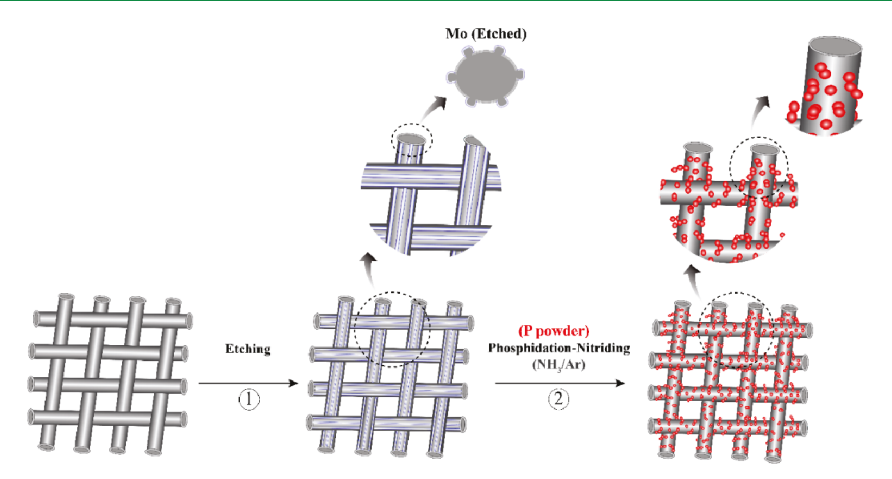


Figure 1. Synthesis path for the Mott-Schottky MoP-Mo2N@Mo heterostructured electrocatalyst (red protrusions are the heterostructure MoP-Mo<sub>2</sub>N formed on the Mo surface).

### EXPERIMENTAL DETAILS

**Synthesis.** Preparation of porous MoPN on Mo meshes. A piece of Mo mesh  $(1 \times 2 \text{ cm}, \sim 0.002 \text{ g}, \text{GOODFELLOW})$ CAMBRIDGE Ltd.) was washed under ultrasonication in propanol and ethanol for 10 min to degrease, and then rinsed with DI water and allowed to dry in an oven at 60  $^{\circ}$ C. The Mo mesh features a thickness of 1 mm and an open area of 75% (40 wire.cm<sup>-2</sup>). The Mo mesh was etched using 5 M hydrochloric acid, and the treatment was carried out at boiling point. After the etching treatment, the mesh was rinsed and dried in the oven at 60 °C for 1 h. Then, the Mo mesh was placed on a quartz boat containing 0.2 g of red phosphorus powder (Sigma-Aldrich, %99.99 pure), where the distance with the powder was kept 1 cm above the powders. After that, the boat and mesh were gently placed inside the quartz tube of the MTI Corporation chemical vapor deposition (CVD) furnace. The tube furnace was kept under vacuum pumping, and Ar was also purged for 10 min at a flow rate of 200 SCCM to evacuate the air and replace it with Ar. The furnace was heated to 800 °C at 10 °C min<sup>-1</sup>, kept at the final temperature for 2 h with purging NH<sub>3</sub>/Ar (1:10 volume ratio) at the flow rate of 25 SCCM, and then cooled down to room temperature at the same rate.

Material Characterization. We utilized various analytical techniques to characterize the structure, phase composition, particle morphology and microstructure, and chemical composition of synthesized Mo-P-N materials. Scanning electron microscopy (SEM) images were collected using a Hitachi S4800 instrument at 10 kV and 15  $\mu$ A. X-ray diffraction (XRD) patterns were obtained by using a Malvern Panalytical Empyrean Nano edition multipurpose X-ray diffractometer. To resolve the peaks in the diffraction pattern, the step size and the integration time were 0.01° and 0.85 s/ step, respectively. A Cu K $\alpha$  X-ray source with a wavelength of 0.154 nm was used for the measurements.

The selected Mo-P-N samples were also examined by high-resolution transmission electron microscopy (HRTEM) to understand the local microstructure and phase. For the TEM sample preparation, an FEI SCIOS FIB/SEM dual beam was employed. The Thermo Scientific Titan Themis probe Cs corrected TEM with a SuperX EDS spectrometer and was used at 200 keV for TEM imaging and elemental color mapping. To further validate the chemical bonding and formation of Mo-P-N in the samples, the same set of samples was probed by

means of Ramana Spectroscopy. The Raman spectroscopic studies were performed on an InVia Micro Raman (Renishaw) spectrophotometer with 532 nm laser excitation. The peaks were fitted following standard procedures, as widely reported in the literature. 41,42 Briefly, Raman spectra were fitted by a superposition of the Lorentzian function:

$$I(\omega) = I_0 \left(\frac{2A}{\pi}\right) \left(\frac{W}{W + 4(\omega - \omega_0)^2}\right) \tag{1}$$

X-ray photoelectron spectroscopic (XPS) scans of the best Mo-P-N electrocatalyst samples were obtained by employing a Thermo Fisher Nexsa spectrometer using Al Klpha monochromatic X-ray source (1486.6 eV) and a high-resolution hemispherical analyzer. The XPS survey and high-resolution scans were recorded with 200 and 50 eV pass energy, and the data obtained were analyzed with the help of CasaXPS software<sup>43</sup> employing Gaussian/Lorentzian (GL(30)) line shape, line asymmetry, and Shirley background correction, which proved to be quite useful for analyzing various cations in complex materials.44-47

Electrochemical Characterization and Performance **Evaluation.** Hydrogen evolution reaction (HER) measurements were carried out on a Solartron analytical-ModuLab Xm workstation using a conventional three-electrode system with Ag/AgCl, Pt mesh (1 cm<sup>2</sup>) as the reference electrode, and the counter electrode, respectively. The prepared electrocatalysts from ultrathin nickel mesh were the working electrodes. The reference electrode was calibrated with respect to a reversible hydrogen electrode (RHE) before experiments. The electrolyte was 0.5 M H<sub>2</sub>SO<sub>4</sub> aqueous solution prepared from DI water. The linear sweep voltammetry (LSV) was recorded at a scan rate of 5 mV s<sup>-1</sup>. Before the LSV measurement, the working electrode was kept at the open circuit potential (OCP) for 60 min to reach a pseudoplato voltage.

The operando electrochemical impedance spectroscopy (Op-EIS) and stability tests were performed simultaneously using fresh electrocatalysts. The electrodes were kept at their OCP for 60 min and then kept under cathodic current of 50 mA for examining the stability of HER activity, while Op-EIS data were collected simultaneously at the same hydrogen evolving potentials with 1 h intervals. The amplitude was 5 mV, while the scan started from 100 kHz to 1 Hz. IR correction was performed to account for the cell resistance

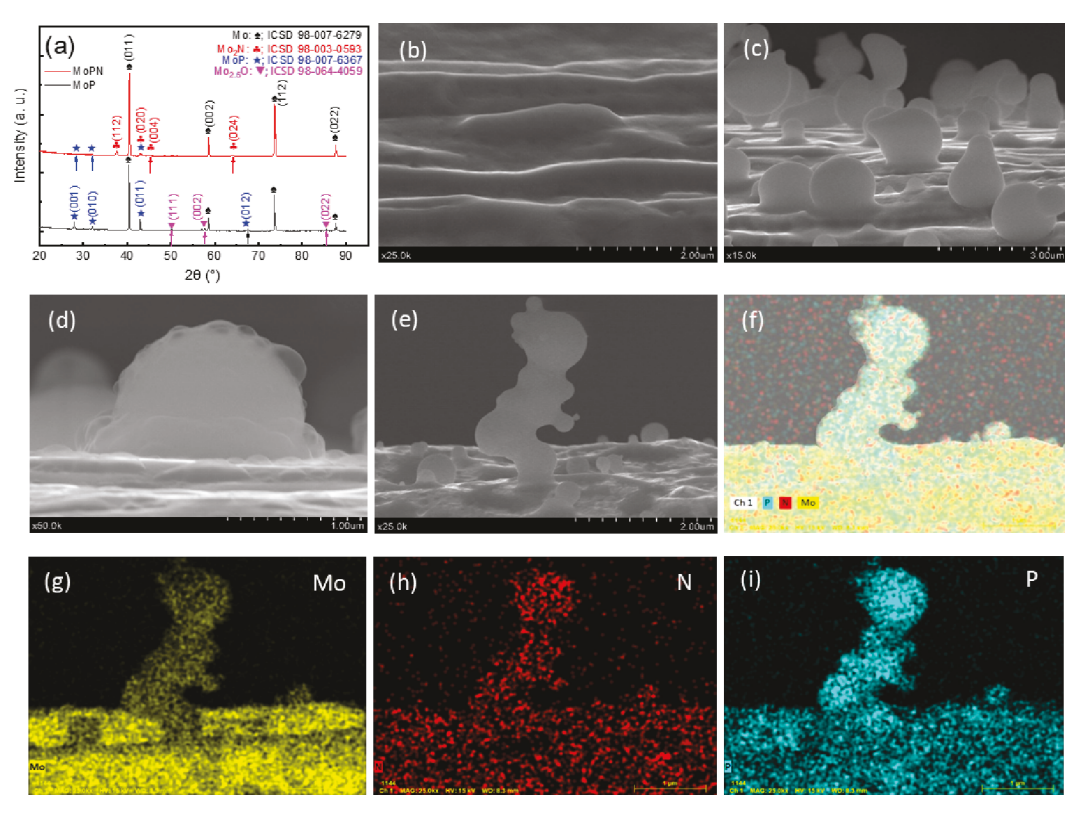


Figure 2. (A) XRD patterns of MoP and MoPN electrodes after phosphidation and phospho-nitriding process, SEM image from (b) etched Mo surface, (c–e) phosopho-nitriding Mo surface for MoPN synthesized at the NH<sub>3</sub>/Ar flow of 25 SCCM, (f–i) elemental mapping from MoPN electrodes for Mo, N, and P elements.

based on the EIS test at the open circuit potential (OCP). Cyclic voltammetry (CV) was also performed at different scan rates ranging from 20 to 200 mV s $^{-1}$  and at the non-Faradaic potential region. We prepared a Pt/C (20%) electrode by using the conventional method. For that, 5 mg of Pt/C (20%) was sonicated for 30 min in 1 mL of solution of ethanol and Nafion (with the 9:1 ratio). We drop-cast the prepared ink on the surface of a glassy carbon electrode. Then, the HER activity of the prepared Pt/C electrode was evaluated under an identical condition in which the synthesized ternary electrocatalysts were tested.

#### RESULTS AND DISCUSSION

Material Characterization. Structural Properties and Chemical Bonding. Figure 1 shows the schematic of the synthesis path for the self-standing MoP and MoPN electrocatalysts. The seamless structures reduce internal resistivity and increase stability by preventing local corrosion. The etching step activates the surface while removing most of the surface oxides, making the surface patterned and suitable for growing the MoP and Mo<sub>2</sub>N protrusions. The formation process of Mo wires is hot extrusion. Therefore, the impact of the extrusion process becomes more apparent after etching using the boiling acid. After rinsing with DI water, the mesh samples are placed inside the chemical vapor deposition (CVD) chamber to employ one-step phospho-nitriding at 800 °C using P powder and purging a mixture flow of NH<sub>3</sub> and Ar (10% of Volume is NH<sub>3</sub>). This process is designed and implemented as previously reported elsewhere.16

X-ray diffraction (XRD) measurements allowed us to recognize the crystalline phases and structural variations of the materials after the first and second steps of synthesis. The

XRD patterns recorded for the MoP and MoPN after phosphidation and phospho-nitriding processes are shown in Figure 2a. For the MoP electrode, it is apparent that MoP forms on the electrode because of obvious characteristic peaks at 27.8°, 31.9°, 42.8°, and 67.2°, being indexed to the (001), (010), (011), and (012) lattice planes of MoP based on ICSD#98-007-6367.<sup>48</sup>

The characteristic diffraction peaks related to Mo are also evident because they are located at 40.5°, 58.6°, and 73.7°, corresponding well to the (011), (002), and (112) planes of cubic Mo based on ICSD#98-007-6279 indicating that Mo remains on the surface and depth of the mesh wires. The lack of complete conversion of Mo to MoP creates the Mott-Schottky electrocatalyst, causing enhanced catalytic performance. A slight amount of oxide remains even after etching in the form of Mo<sub>2.5</sub>O on the surface, with the characteristic peaks at 50.5°, 59°, and 88.3° representing the (111), (002), and (022) planes. For the MoPN electrode, we can recognize three phases of MoP, Mo<sub>2</sub>N, and the remaining Mo from the XRD analyses. The characteristic peaks related to the tetragonal crystal of the Mo<sub>2</sub>N phase are located at 37.7°,  $43^{\circ}$ ,  $45.3^{\circ}$ , and  $64.2^{\circ}$  corresponding to the (112), (020), (004), and (024) planes based on ICSD#98-003-0593. 49 Therefore, we can deduce that the phospho-nitriding process on the Mo mesh can create the Mott–Schottky MoP–Mo<sub>2</sub>N@ Mo heterostructured electrocatalysts. Thus, the XRD data validate and correlate with the proposed mechanism (schematic representation; Figure 1) for the formation of MoP-Mo<sub>2</sub>N@Mo compounds upon one-step treatment.

Raman spectroscopy gives information about chemical bonds and changes in the crystal structure with the substitution of certain ions in the lattice. It is extremely sensitive to the local structure and chemical bonding. 20,24 Therefore, we used Raman spectroscopy measurements on the Mo-P-N sample to study the chemical bonding in the Mo-P-N complex nanocomposite material. Figure S1 shows the Raman spectrum from the high to midfrequency range, whereas Figure S2 depicts the high-resolution scan for the low wavenumber range. A total of seven peaks are identified here as Raman active lattice vibration modes: 165, 226, 357, 502, 711, 891, and 957 cm<sup>-1</sup>. The broad short wavenumber peaks (165, 226 cm<sup>-1</sup>) attributed to the Mo-N acoustic branches, 50 namely the longitudinal (LA) and transverse (TA) branches. The small peak at 357 cm<sup>-1</sup> represents the terminal Mo=O bending modes. 51 The broad peak at 711 cm<sup>-1</sup> can be ascribed to the presence of triply coordinated oxygen Mo<sub>3</sub>-O.<sup>52</sup> The peak at 502 cm<sup>-1</sup> corresponds to Mo-O, s3 while the midfrequency peaks at 891 and 957 cm<sup>-1</sup> correspond to Mo-P.<sup>54</sup>

Surface Chemistry, Morphology, and Microstructure. To further characterize the structure and surface morphology of developed electrodes, we used scanning electron microscopy (SEM) and elemental mapping using energy dispersive spectroscopy (EDS). In Figure 2b, the surface morphology of the Mo electrode after the etching process in the boiling solution of 3 M chloride acid can be observed. For comparison, the SEM data of Mo before the etching process are shown in Figure S3. The parallel lines on the surface (Figure 2b) are an indication of lines formed during the hot extrusion process of Mo wires, where the etching process significantly intensifies their appearance on the surface. After the phosphonitriding process, SEM images in Figure 2c indicate the formation of spherical hierarchies on the surface. The magnified SEM image in Figure 2d illustrates a semispherical shape forming on the surface, indicating a gradual formation of spherical hierarchies on the surface, where the continuation of the growth process results in either bigger spheres or a hierarchy formation, as shown in Figure 2e. The EDS elemental mapping analyses from the hierarchies are shown in Figure 2f-i. The EDS spectra and mapping analyses can validate the chemical homogeneity and elemental composition since the X-ray energy is a property of the specific atom(s) that is/are involved in the generation of the X-rays. \$5,56 Thus, the presence of both P and N along with Mo suggests contribution of both MoP and Mo2N phases in the formed hierarchies. The phase modulation of the complex material with multiple anions may also involve interfacial stress,<sup>57</sup> which may also be beneficial to enhance the electrochemical property.

The TEM data in Figure 3 provide compelling evidence of the distinct nanostructural characteristics that emerge following the phosphidation and phosphor-nitriding processes. Specifically, these TEM images illustrate the growth of Mo-P-N nanostructures around the periphery of Mo. Figure 3a-c displays high-resolution transmission electron microscopy (HRTEM) images captured from two different locations surrounding the MoPN nanostructures, as shown by the red marks. Calculated d-spacing at different positions indicates the mixed existence of Mo<sub>2</sub>N and MoP with different crystallographic orientations. Assertively, the corresponding reciprocal space, 16,58,59 simulated by Fast-Fourier Transform (FFT; Figure 3d), shows paired spots rather than single bright spots (indicated by the blue circle), which supports the existence of mixed phases and the formation of Mo<sub>2</sub>N-MoP nanocomposite. Additionally, the STEM-EDS color mapping (Figure S4) clearly shows the characteristics of the Mo-MoPN interface. The existence of Ga at the top layer is due to

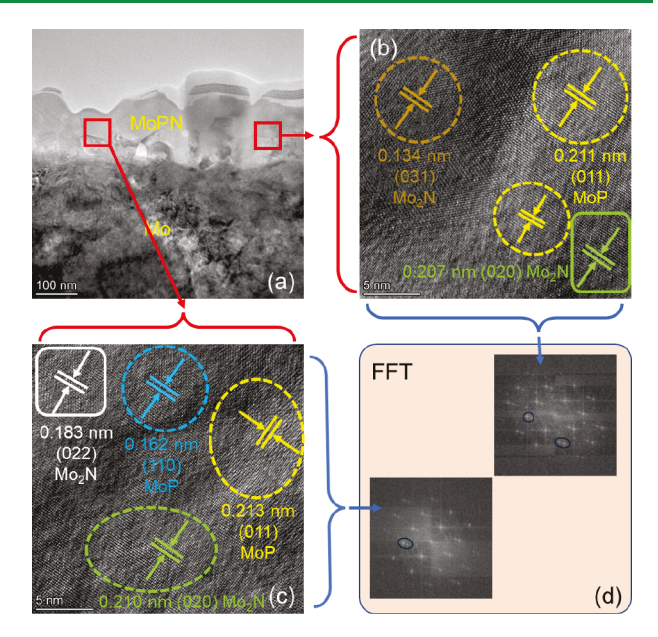


Figure 3. (a) The TEM images of the  $MoP-Mo_2N/Mi$  heterostructure, (b, c) the magnified high-resolution TEM images, and (d) FFT of the selected regions. The spacing between lattice fringes and corresponding diffraction patterns (FFT) indicate the coexistence of  $Mo_2N$  and MoP phase intact with each other.

the FIB and TEM sample preparation process. 58,59 Further, the STEM-EDS data also corroborate the SEM-EDS data, as presented in Figure 2. Thus, the TEM characterization and detailed structural and chemical evaluations make it clear that the growth process resulted in transition metal phosphide nanocomposite nanostructures with specific alloying of nitrides.

X-ray photoelectron spectroscopy (XPS) is a valuable analytical tool to characterize and investigate the surface chemistry and electronic properties of the electrocatalysts. We used XPS on the Mo-based electrocatalysts before and after electrochemical performance to exhibit their unique electronic structure and surface chemistry. The application of XPS in the analysis of Mo-based electrocatalysts offers insights into the changes in the surface composition, chemical states, and binding energies of species, providing a fundamental understanding of their catalytic mechanisms and contributing to the development of efficient electrochemical energy conversion devices. In this context, we employ MoP and MoPN<sub>2</sub> electrocatalysts to explore their XPS analyses with the use of CasaXPS software. 43 We studied these electrodes after their syntheses and the changes that may occur after catalytic performance. Therefore, we can verify the formation of Mo<sub>2</sub>N-MoP heterostructure in the Mo<sub>2</sub>N-MoP@Mo superstructure using the Mo 3d, N 1s, and P 2p characteristic peaks of two developed electrodes. 49,60

The XPS results obtained at selected times for both electrocatalysts are presented in Figure 4. As shown in Figure 4a, the core-level XPS spectra for Mo 3d display peaks at the binding energy (BE) of 232.11, 230.36 eV and 228.92 eV for the MoPN electrocatalyst, respectively, characterizing the existence of Mo ions in Mo<sup>6+,</sup> Mo<sup>4+</sup>, and Mo<sup>2+</sup> states. The peak observed at a binding energy of 233.4 eV corresponds to the S 2s peak. It is clear from the figure that a majority of the Mo ions in the as-synthesized sample exist in the Mo<sup>4+</sup> states. However, upon catalytic activity for 24 h (bottom panel in

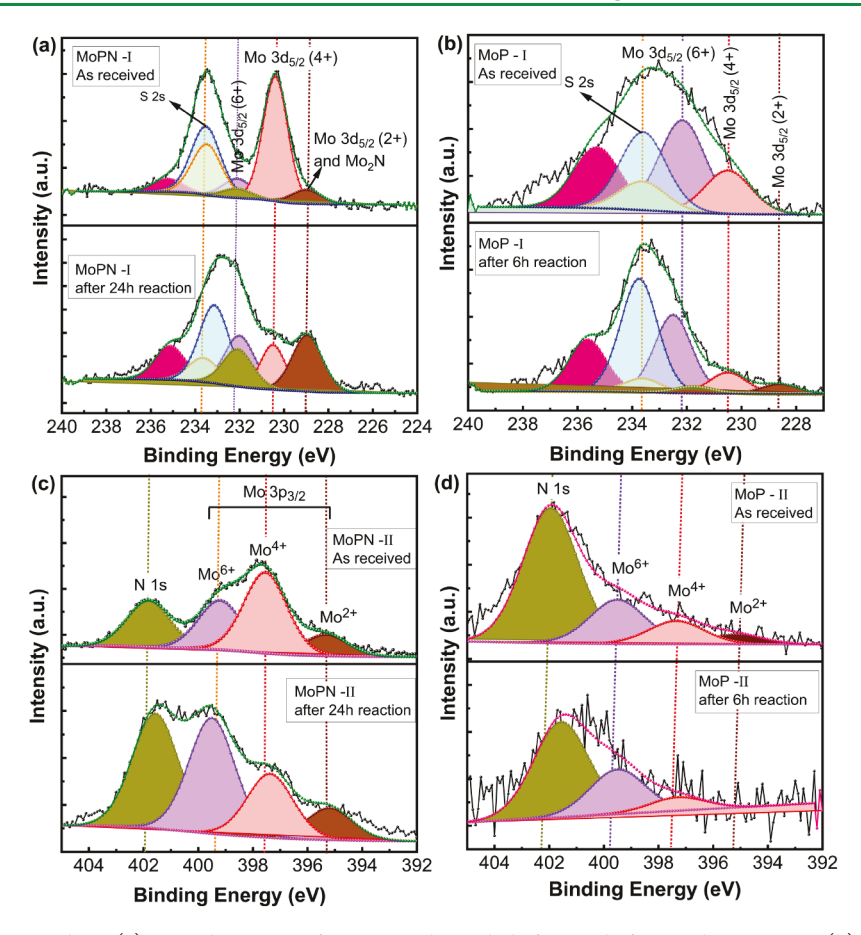


Figure 4. XPS results corresponds to (a) Mo 3d spectrum for MoNP electrode before and after catalytic activity, (b) Mo 3d spectrum for MoP electrode before and after catalytic activity, (c) Mo  $3p_{3/2}$  spectrum for MoPN electrode before and after catalytic activity, (d) Mo  $3p_{3/2}$  spectrum for MoP electrode before and after catalytic activity.

Figure 4a), it becomes apparent that the contribution of Mo<sup>6+</sup> and Mo<sup>2+</sup> has increased while the Mo<sup>4+</sup> content has decreased. This observation clearly indicates that both oxidation and reduction reactions occur at the surface during catalytic activity. On the other hand, the Mo 3d spectra shown in Figure 4b from the MoP sample reveal a mixed state of Mo4+ and Mo<sup>6+</sup> exist, with Mo<sup>6+</sup> amount is slightly higher than Mo<sup>4+</sup>. After 6 h of catalytic activity, a marginal increase in Mo<sup>6+</sup> is observed. Notably, Mo<sup>2+</sup> states are absent in the MoP sample following catalytic activity, suggesting that only the oxidation reaction occurs at the surface of the MoP sample. We later explain the details of the catalytic activity of these materials in the subsequent (electrochemical) section. Figure 4c and d exhibits the binding energy regions of N 1s and Mo 3p<sub>3/2</sub> photoelectron peaks for both MoPN and MoP samples. Mo 3p data from the MoPN sample agrees well with the Mo 3d XPS data.

The increase in the Mo<sup>2+</sup> states in the MoPN sample after catalytic activity can be attributed to several factors. Catalytic activity often involves the interaction of reactant molecules with the catalyst surface, leading to changes in the electronic structure of the catalyst. When reactant molecules adsorb onto the catalyst surface, they can interact with the Mo atoms, leading to electron transfer between the catalyst and reactant. This electron transfer can cause a shift in the binding energy of the Mo 3d electrons. Catalytic reactions can also induce changes in the oxidation state of the metal atoms in the catalyst. For example, Mo can undergo oxidation or reduction

during a catalytic process. The change in the oxidation state can also influence the electronic environment around the Mo atoms, resulting in a shift in the BE of the Mo 3d electrons.<sup>63</sup> Catalytic reactions can induce surface reconstruction of the catalyst, where the arrangement of atoms on the surface undergoes changes. This reconstruction can lead to alterations in the local environment around the Mo atoms, affecting their binding energy. 38,49,64,65 During catalytic activity, new chemical species can form on the catalyst surface, such as adsorbed intermediates or reaction products. These surface species can interact with the Mo atoms and modify their electronic properties, leading to a shift in the binding energy of the Mo 3d electrons. 66 Overall, the emergence of Mo<sup>2+</sup> for the MoPN electrocatalyst after 24 h of catalytic activity is a reflection of the surface reconstruction and results in greater stability of the catalyst with a prolonged performance due to the changes in the electronic structure and chemical environment of the catalyst.

The XPS fitting suggests that theMoPN2 electrocatalyst shows both reduction and oxidation after 24 h of the HER performance, while the MoP electrocatalyst shows only an oxidation process after 6h of the catalytic activity. These results agree with layer-structured electrocatalytic compounds, such as MoPN2, undergoing a reconstruction process during the HER performance that changes in the oxidation states can improve the conductivity, leading to prolonged stability can be obtained.

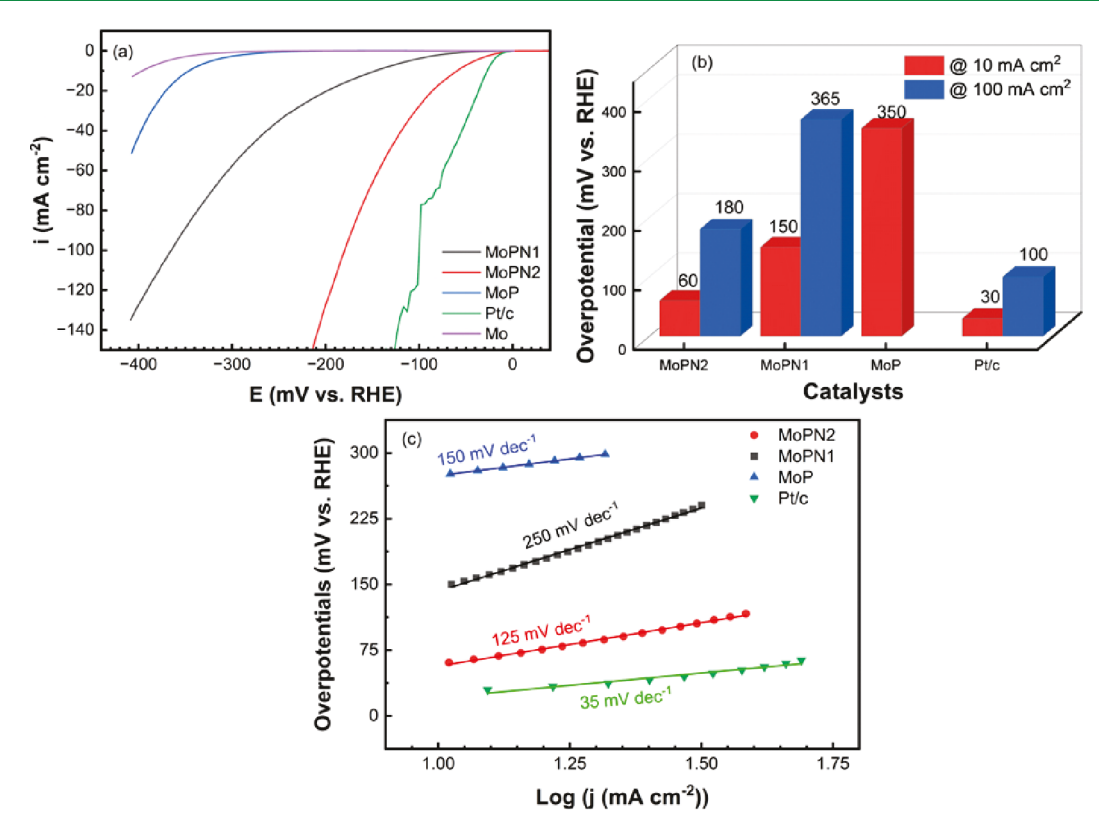


Figure 5. (a) IR-corrected linear sweep voltammetry (LSV) for HER performance, (b) 3D bar chart for overpotential profiles of the developed catalysts, and (c) Tafel slope plots for the developed electrocatalysts.

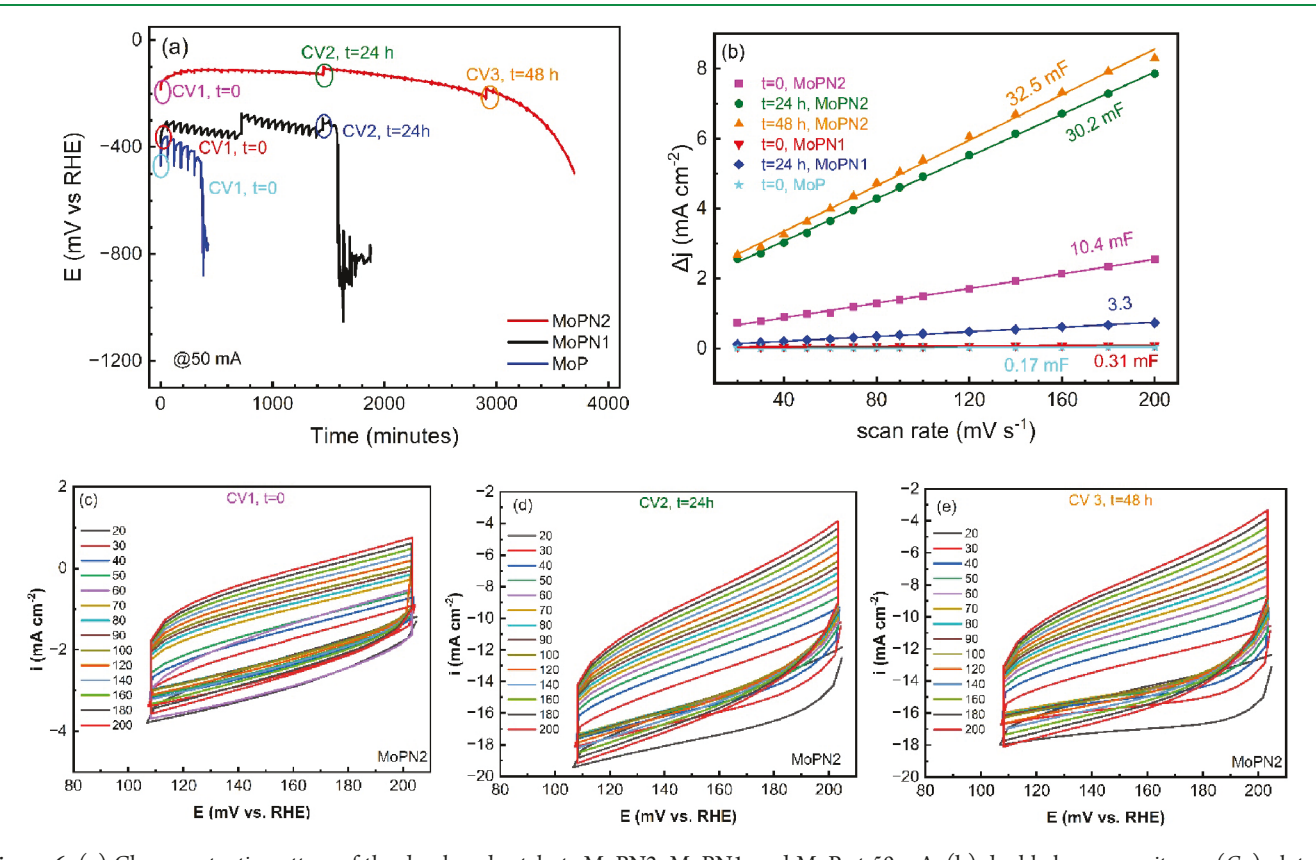


Figure 6. (a) Chronopotentiomettery of the developed catalysts MoPN2, MoPN1, and MoP at 50 mA, (b) double-layer capacitance ( $C_{\rm dl}$ ) plot of the catalysts corresponding to the stability time, and (c-e) cyclic voltammetry of the MoPN2 catalyst at t = 0, 24, and 48 h corresponding to the stability time.

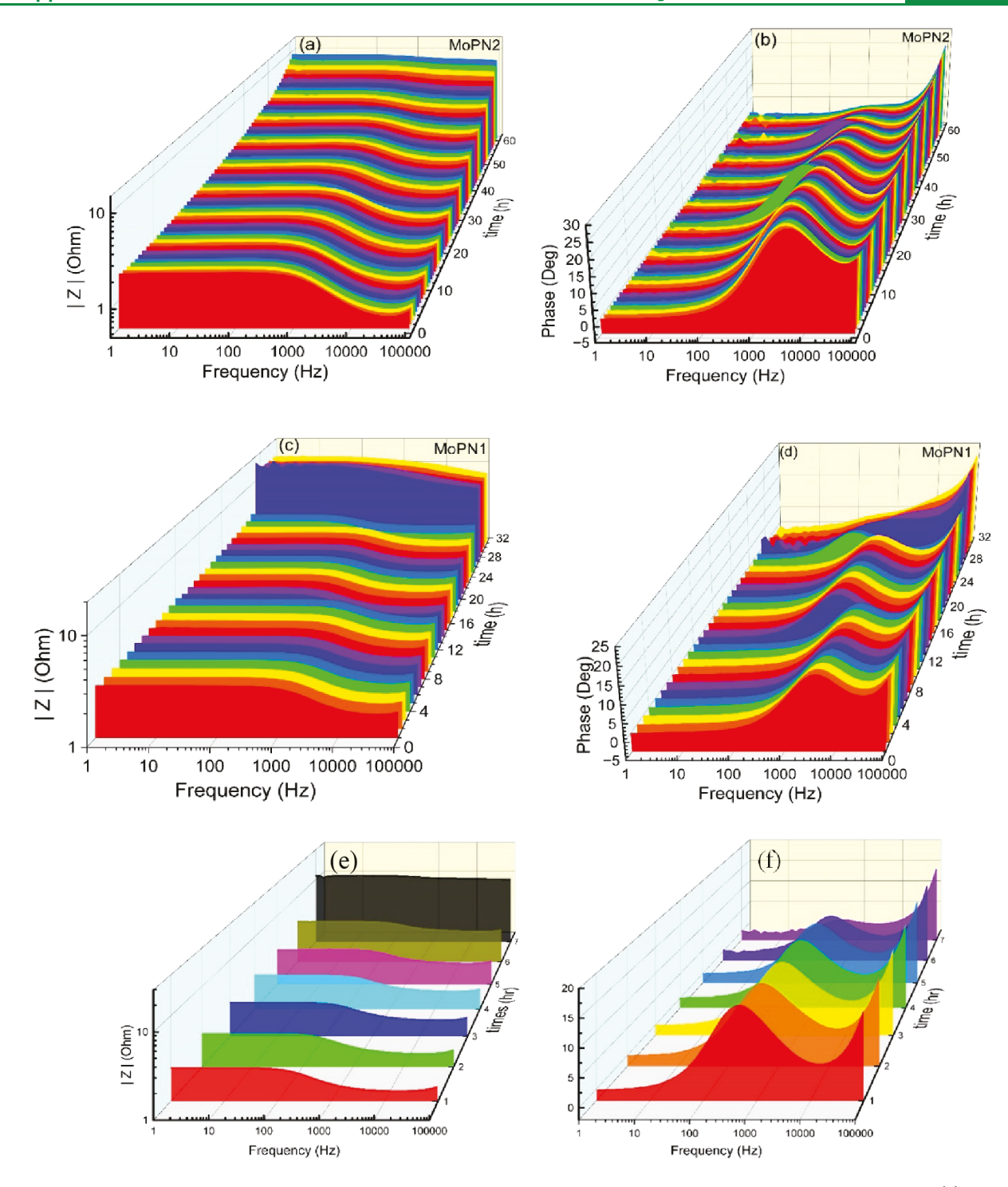


Figure 7. Operando EIS is illustrated by Bode |Z| and Bode phase graphs. The data shown are illustration of Op–EIS results fo:r (a) Bode |Z| of MoPN2, (b) Bode phase of MoPN2, (c) Bode |Z| of MoPN1, (d) Bode phase of MOPN1, (e) Bode Z of MoP, and (f) Bode phase of MoP electrodes.

Electrochemical Evaluation Voltammetry. The electrocatalytic HER performances of the MoP-Mo<sub>2</sub>N@Mo (MoPN1, 2), MoP-Mo<sub>2.5</sub>O@Mo (MoP), and commercial 20 wt % Pt/C are investigated to determine the role of inducing nitrogen into the MoP crystal structure on the performance and durability of the developed catalysts. The HER activities are examined in an Ar (Ar) saturated 0.5 M sulfuric acid solution using three electrode compartments, where Pt mesh (1 cm²) and Ag/AgCl are the auxiliary and

reference electrodes, respectively. The working electrode is the synthesized catalyst with an area of 1 cm². The electrocatalytic current density is normalized by considering the catalyst geometry and active surface area. The IR-corrected linear sweep voltammetry (LSV) at a scan rate of 2 mV s $^{-1}$  is shown in Figure 5a. It indicates that the Mott–Schottky MoP–Mo $_2$ N@Mo (MoPN2) heterostructured electrocatalyst is the champion catalyst with the lowest overpotential. As shown by the LSV plots, developing the Mott–Schottky system and

generating a heterostructure can be the reason behind boosting the electrocatalytic activity, where the overpotentials for the MoPN2 catalyst are 60 and 180 mV to attain current densities of 10 and 100 mA cm<sup>-2</sup>, respectively. The 3D bar chart in Figure 5b displays the overpotential values, and the values for the champion catalyst are decent compared to the commercial Pt/C catalyst.<sup>67</sup> Even though the obtained overpotentials do not beat values for the commercial Pt/C catalysts, this study is meant to show the importance of inducing the second nonmetal element in modifying the durability and stability of an electrocatalyst. Based on the work of Murthy et al., we used a linear fitting method on the polarization curves to obtain the Tafel slopes. 88 The HER kinetics of the electrocatalysts are reflected by the Tafel slopes in Figure 5c. The plots show that the intrinsic catalytic activity is enhanced for the MoP-Mo<sub>2</sub>N@Mo catalysts, where MoPN2 shows the value of 125  $mV dec^{-1}$ .

The stability and durability of the electrocatalysts are the key concern. 18,19 To assess the HER stability of the synthesized materials, we apply a current of 50 mA to the electrodes and present their chronopotentiometry plots in Figure 6a. This type of durability test is designed to represent the continuous electrolysis reaction of water with low currents. The MoP catalyst shows an abrupt change in its overpotential after 7 h. Cyclic voltammetry is carried out in the cathodic voltage range with the scanning rates of (20–200 mV s<sup>-1</sup>) (noted by CV1 in cyan color, shown Figure 6a) is performed while the MoP electrocatalyst was kept for 1 h in the open circuit potential and before initiating catalytic activity, which we call it "time zero", t = 0. The double layer capacitance ( $C_{dl}$ ) for the MoP electrocatalyst is measured and displayed in Figure 6b, 0.17 mF. Likewise, the stability test is carried out for MoPN1 and MoPN2 electrocatalysts. For MoPN2, the longest stability for the catalytic HER performance is recorded. Cyclic voltammetry in the same cathodic voltage range with scanning rates of  $(20-200 \text{ mV s}^{-1})$  is performed three times with 24 h intervals. For the MoPN1 electrocatalyst, two CVs are recorded with 24 h intervals based on its stability performance, which are noted by red and blue colors in Figure 6a. Figure 6c-e shows these three CVs which are noted by purple, green, and orange colors in Figure 5a, during the stability test for MoPN2 to realize the change of double layer capacitance. The plots and measured double layer capacitances  $(C_{\rm dl})$  for these three intervals are displayed with the same color in Figure 6b. As is evident, C<sub>dl</sub> increases significantly at t = 24 and 48 h. The expansion in CVs with time and obtained  $C_{\rm dl}$  indicates that the electrochemical surface area (ECSA) increases during catalytic HER performance. Figure 6b shows that the  $C_{\rm dl}$  for MoPN2 varies from 10.4 to 32.5 mF. As it seems, there can be a relation between surface reconstruction and variation in the double layer capacitance in certain electrochemical systems. In fact,  $C_{\rm dl}$  is related to the charge accumulation at the interface between an electrode and an electrolyte. It is influenced by the surface properties of the electrode, including its structure, composition, and active sites. Surface reconstruction refers to the rearrangement of atoms or molecules on the surface of a material, leading to changes in its surface structure and morphology. This phenomenon can occur due to various factors such as chemical reactions, adsorption/desorption processes, or exposure to reactive species. Therefore, the variation in double layer capacitance can be attributed to the surface reconstruction phenomena for several reasons, such as surface area changes, increased exposure at active sites, and increased surface coverage and

electrolyte accessibility. An increase in the surface area can result in a higher double layer capacitance due to more available sites for charge accumulation. Surface reconstruction may also expose new active sites or alter the distribution of existing active sites on the electrode surface. This can affect the kinetics of charge transfer processes at the electrodeelectrolyte interface and influence the double layer capacitance. In addition, some surface reconstruction processes may result in the formation of new adsorbates or species on the electrode surface. These adsorbates can affect the formation of electric double layers and alter the double layer capacitance. It is worth noting that changes in surface reconstruction can modify the accessibility of the electrolyte to the electrode surface. This can impact ion diffusion and charge accumulation in the electric double layer, leading to variations in the double layer capacitance. The relation between surface reconstruction and variation in double layer capacitance is a complex subject and an active area of research, particularly in the field of electrocatalysis and energy storage materials. Experimental techniques, such as electrochemical impedance spectroscopy (EIS), are valuable tools to study and quantify these effects.

Operando Electrochemical Impedance Spectroscopy. Operando electrochemical impedance spectroscopy (Op-EIS) offers several significant advantages in the assessment of the stability of the HER electrocatalysts. Op-EIS allows for real-time monitoring of the electrochemical performance of the HER electrocatalyst during the catalytic reaction. This provides valuable insights into the dynamic changes in the catalyst's behavior, which are not captured in static ex situ measurements. It enables us to observe the catalyst's stability under realistic operating conditions, which is crucial for evaluating its long-term performance. By continuously monitoring the impedance response during the HER, Op-EIS can identify changes in the electrochemical behavior that may indicate degradation mechanisms or poisoning effects. This information is essential for understanding electrocatalyst deactivation and designing more stable materials. In fact, Op-EIS also provides mechanistic insights into the electrochemical processes occurring at the catalyst-electrolyte interface during HER. This deeper understanding can lead to the design of improved catalysts with enhanced stability and activity. As shown in Figure 7a,b, the 3D profile of Bode |Z| and Bode phase changes with time and provides valuable information about increasing the electrocatalyst resistance and the shift of the apex degree versus the frequency with time for MoPN2 electrocatalysts. The gradual increase during catalytic activity indicates that degradation occurs with increasing resistance at higher frequencies. Noticeably, the apex in the Bode phase plot in Figure 7b shifts to higher frequency, indicating that the charge transfer resistance decreases and the double layer capacitance increases gradually with time, which is more significant after 24 h of catalytic performance. These results confirm the earlier presented XPS studies on the valences change with time, where we realize that the Mo<sup>2+</sup> appears after 24 HER performance and the amount of Mo<sup>6+</sup> decreases. On the contrary, the charge transfer resistance rises abruptly after 6 h for the MoP electrode. This noticeable change is consistent with the change of recorded voltages in Figure 6a, where it shows the electrocatalyst degradation for the MoP electrocatalyst. The apex in the Bode phase plot shifts to lower frequencies with time, indicating that the double layer capacitance decreases with time. Therefore, the MoPN2 electrode exhibits a reconstruction behavior during catalytic activity, where the

intrinsic catalytic activity modifies with time and hydrogen evolution enhances with time, as confirmed by CVs and Op-EIS studies.

Finally, we examine the function of different phases and their role to bring the mechanistic elements into focus, in order to shed light on the overall electrochemical activity and stability of the multiphase, heterostructured catalysts. The roles of MoP, Mo<sub>2</sub>N, and Mo phases can be elaborated regarding the structure and electrochemical behavior of the electrocatalyst. The LSV plot in Figure 5a shows the electrochemical behavior of the Mo electrode, where its high overpotential (~400 mV @ 10 mA) implies a weak electrocatalytic behavior. Therefore, the Mo electrode performing electrocatalytic hydrogen evolution degrades in a short time. The MoP phase obtained on the Mo electrode is synthesized by only a phosphidation process. This electrode does not show any hierarchical features on the surface. The MoP electrode is examined for electrocatalytic performance. The weak catalytic performance of the Mo electrode motivates us for the phosphidation and nitriding treatments. After inducing the phosphor element and the formation of MoP on the surface of the Mo mesh, the electrocatalytic behavior is improved, which can be attributed to the creation of the MoP on the surface. However, the electrode suffers a lack of stability, where the HER catalytic performance diminishes in a relatively short time. Therefore, the formation of the MoP phase only improves the catalytic behavior compared to that of the Mo phase. The Mo phase existing in the core of the electrocatalysts provides general mechanical stability and transfers charges to the catalyst phases. Remarkably, we notice the formation of a 3D structure on the MoPN2 electrode, indicating this feature is generated only after the simultaneous phosphidation and nitridationcontrolled process. The Mo<sub>2</sub>N phase enhances the intrinsic catalytic behavior, where both the overpotential and Tafel slope decrease significantly as shown in Figure 5 for the MoPN2 electrode. The expansion of CV plots for the MoPN2 electrode and the increase of  $C_{\text{dl}}$  indicate an increase in the electrochemical surface area (ECSA), in which a more active catalytic surface is provided for the HER performance. The remarkable decrease in the charge transfer resistance obtained from the EIS results also indicates that the Mo2N phase amplifies the charge mobility at the interfaces between the H intermediates and the electrocatalyst surface, where the HER performance improves significantly for the MoPN2 electrode. The stability study of the prepared electrocatalysts reveals that the durability improves remarkably for the MoPN2 electrode. Therefore, the role of the Mo<sub>2</sub>N phase can be identified as strengthening the durability of the electrocatalyst by providing a reconstruction mechanism and enhancing the charge mobility at the interfaces. The Mo<sub>2</sub>N phase increases the longevity of the HER performance in an acidic electrolyte and improves the intrinsic catalytic characteristics. The seamless MoPN2 electrode contains hierarchical MoP-Mo2N semispheres that increase the electrochemically active surface area and provide charge transfer at the interfaces.

# CONCLUSIONS

The heterostructures of MoP-Mo2N@Mo electrocatalysts were synthesized in a one-step phospho-nitriding process. The 3D structure and heterostructure of the catalysts participate in durability and stability of the electrocatalyst in longer times. The catalytic performance shows a low overpotential of 65 and 180 mV to attain the current density of 10 and 100 mA cm<sup>2-</sup>,

where the Tafel slope also indicates enhancing the intrinsic catalytic activity of the MoP-Mo2N@Mo electrocatalyst. The stability test indicates longer durability of electrocatalyst and gradual degradation of the catalyst with increasing resistance at higher frequencies.

# **ASSOCIATED CONTENT**

# Supporting Information

The Supporting Information is available free of charge at https://pubs.acs.org/doi/10.1021/acsami.3c14160.

The Supporting Information (SI) includes additional details and data of the materials. The specific details are Ramana spectroscopic data of Mo-P-N samples, peakfitting analyses of Raman spectroscopic data, SEM data of as received or pre-etched Mo, and STEM-EDS mapping data of Mo-P-N nanomaterials. (PDF)

#### AUTHOR INFORMATION

### **Corresponding Author**

C.V. Ramana - Centre for Advanced Materials Research (CMR) and Department of Aerospace & Mechanical Engineering, University of Texas at El Paso, El Paso, Texas 79968, USA; Environmental Molecular Sciences Laboratory (EMSL), Pacific Northwest National Laboratory (PNNL), Richland, Washington 99352, USA; Email: rvchintalapalle@utep.edu

#### **Authors**

Navid Attarzadeh - Centre for Advanced Materials Research (CMR) and Environmental Science and Engineering, University of Texas at El Paso, El Paso, Texas 79968, USA; orcid.org/0000-0002-3460-326X

Ambadi Lakshmi-Narayana – Centre for Advanced Materials Research (CMR), University of Texas at El Paso, El Paso, Texas 79968, USA

Debabrata Das - Centre for Advanced Materials Research (CMR), University of Texas at El Paso, El Paso, Texas 79968, USA; o orcid.org/0000-0003-4326-6805

Susheng Tan - Department of Electrical and Computer Engineering and Petersen Institute of NanoScience and Engineering, University of Pittsburg, Pittsburgh, Pennsylvania 15261, USA; orcid.org/0000-0002-6162-7443

Vaithiyalingam Shutthanandan - Centre for Advanced Materials Research (CMR), University of Texas at El Paso, El Paso, Texas 79968, USA; Environmental Molecular Sciences Laboratory (EMSL), Pacific Northwest National Laboratory (PNNL), Richland, Washington 99352, USA; orcid.org/0000-0003-2957-7535

Complete contact information is available at: https://pubs.acs.org/10.1021/acsami.3c14160

The authors declare no competing financial interest.

# **ACKNOWLEDGMENTS**

The authors acknowledge, with pleasure, support from the National Science Foundation (NSF) with NSF-PREM grant #DMR-1827745. A portion of this research (Chemical Composition Analyses using X-ray Photoelectron Spectroscopy) was performed on a project award (10.46936/cpcy.proj.2021.60259/60008213) from the Environmental Molecular Sciences Laboratory, a DOE Office of Science User

Facility sponsored by the Biological and Environmental Research program under Contract No. DE-AC05-76RL01830 and also funded in part by a grant from the Washington State Department of Commerce's Clean Energy Fund. A portion of the research was supported by the UTEP-PNNL Laboratory Research and Development Project (LDRD) initiative at PNNL. CVR and VS sincerely acknowledge the UTEP-PNNL LDRD project support and resources for facilitating collaborative research.

# REFERENCES

- (1) van Renssen, S. The hydrogen solution? *Nat. Clim. Change* **2020**, 10, 799–801.
- (2) Ahmed, S. F.; Mofijur, M.; Nuzhat, S.; Rafa, N.; Musharrat, A.; Lam, S. S.; Boretti, A. Sustainable hydrogen production: Technological advancements and economic analysis. *Int. J. Hydrog. Energy* **2022**, *47*, 37227–37255.
- (3) Mneimneh, F.; Ghazzawi, H.; Abu Hejjeh, M.; Manganelli, M.; Ramakrishna, S. Roadmap to Achieving Sustainable Development via Green Hydrogen. *Energies* **2023**, *16*, 1368.
- (4) Vesborg, P. C. K.; Seger, B.; Chorkendorff, I. Recent Development in Hydrogen Evolution Reaction Catalysts and Their Practical Implementation. *J. Phys. Chem. Lett.* **2015**, *6*, 951–957.
- (5) Zhang, X.; Wang, J.; Liu, D.; Zhang, Y.; Chu, P. K.; Zhou, Z.-Y.; Yu, X.-F. Insight into the overpotentials of electrocatalytic hydrogen evolution on black phosphorus decorated with metal clusters. *Electrochim. Acta* **2020**, 358, 136902.
- (6) Hou, C.; Tai, G.; Liu, Y.; Wu, Z.; Liang, X.; Liu, X. Borophene-based materials for energy, sensors and information storage applications. *Nano Res. Energy* **2023**, *2*, No. e9120051.
- (7) Zhang, L.; Han, L.; Liu, H.; Liu, X.; Luo, J. Potential-Cycling Synthesis of Single Platinum Atoms for Efficient Hydrogen Evolution in Neutral Media. *Angew. Chem., Int. Ed.* **2017**, *56*, 13694–13698.
- (8) Luo, X.; Zhou, Q.; Du, S.; Li, J.; Zhang, L.; Lin, K.; Li, H.; Chen, B.; Wu, T.; Chen, D.; Chang, M.; Liu, Y. One-Dimensional Porous Hybrid Structure of Mo<sub>2</sub>C-CoP Encapsulated in N-Doped Carbon Derived from MOF: An Efficient Electrocatalyst for Hydrogen Evolution Reaction over the Entire pH Range. ACS Appl. Mater. Interfaces 2018, 10, 42335–42347.
- (9) Zhang, Q.; Xia, T.; Huang, H.; Liu, J.; Zhu, M.; Yu, H.; Xu, W.; Huo, Y.; He, C.; Shen, S.; Lu, C.; Wang, R.; Wang, S. Autocatalytic reduction-assisted synthesis of segmented porous PtTe nanochains for enhancing methanol oxidation reaction. *Nano Res. Energy* **2023**, *2*, No. e9120041.
- (10) Groves, M. N.; Malardier-Jugroot, C.; Jugroot, M. Improving Platinum Catalyst Durability with a Doped Graphene Support. *J. Phys. Chem. C* **2012**, *116*, 10548–10556.
- (11) Zhao, G.; Rui, K.; Dou, S. X.; Sun, W. Heterostructures for Electrochemical Hydrogen Evolution Reaction: A Review. *Adv. Funct. Mater.* **2018**, 28, 1803291.
- (12) Liu, Z.; Nie, K.; Qu, X.; Li, X.; Li, B.; Yuan, Y.; Chong, S.; Liu, P.; Li, Y.; Yin, Z.; Huang, W. General Bottom-Up Colloidal Synthesis of Nano-Monolayer Transition-Metal Dichalcogenides with High 1T'-Phase Purity. *J. Am. Chem. Soc.* **2022**, *144*, 4863–4873.
- (13) Wang, L.; Qi, G.; Liu, X. Sulfur dopant-enhanced neutral hydrogen evolution performance in MoO<sub>3</sub> nanosheets. *Nanotechnology* **2022**, *33*, 065701.
- (14) Yao, N.; Meng, R.; Su, J.; Fan, Z.; Zhao, P.; Luo, W. Dual-phase engineering of MoN/Co<sub>4</sub>N with tailored electronic structure for enhanced hydrogen evolution. *Chem. Eng. J.* **2021**, *421*, 127757.
- (15) Pi, C.; Huang, C.; Yang, Y.; Song, H.; Zhang, X.; Zheng, Y.; Gao, B.; Fu, J.; Chu, P. K.; Huo, K. In situ formation of N-doped carbon-coated porous MoP nanowires: a highly efficient electrocatalyst for hydrogen evolution reaction in a wide pH range. *Appl. Catal. B* **2020**, 263, 118358.
- (16) Attarzadeh, N.; Das, D.; Chintalapalle, S. N.; Tan, S.; Shutthanandan, V.; Ramana, C. V. Nature-Inspired Design of Nano-Architecture-Aligned Ni<sub>5</sub>P<sub>4</sub>-Ni<sub>2</sub>P/NiS Arrays for Enhanced Electro-

- catalytic Activity of Hydrogen Evolution Reaction (HER). ACS Appl. Mater. Interfaces 2023, 15, 22036–22050.
- (17) Wang, X.; Tai, G.; Wu, Z.; Hu, T.; Wang, R. Ultrathin molybdenum boride films for highly efficient catalysis of the hydrogen evolution reaction. *J. Mater. Chem. A* **2017**, *5*, 23471–23475.
- (18) Xu, M.; Wang, R.; Bian, K.; Hou, C.; Wu, Y.; Tai, G. Triclinic boron nanosheets high-efficient electrocatalysts for water splitting. *Nanotechnology* **2022**, *33*, 075601.
- (19) Tai, G.; Xu, M.; Hou, C.; Liu, R.; Liang, X.; Wu, Z. Borophene Nanosheets as High-Efficiency Catalysts for the Hydrogen Evolution Reaction. ACS Appl. Mater. Interfaces 2021, 13, 60987–60994.
- (20) Ramana, C. V.; Mauger, A.; Julien, C. M. Growth, characterization and performance of bulk and nanoengineered molybdenum oxides for electrochemical energy storage and conversion. *Prog. Cryst. Growth Charact. Mater.* **2021**, *67*, 100533.
- (21) Ramana, C. V.; Atuchin, V. V.; Groult, H.; Julien, C. M. Electrochemical properties of sputter-deposited MoO<sub>3</sub> films in lithium microbatteries. *J. Vac. Sci. Technol. A* **2012**, *30*, 04D105.
- (22) Kwak, D.; Wang, M.; Koski, K. J.; Zhang, L.; Sokol, H.; Maric, R.; Lei, Y. Molybdenum Trioxide ( $\alpha$ -MoO<sub>3</sub>) Nanoribbons for Ultrasensitive Ammonia (NH<sub>3</sub>) Gas Detection: Integrated Experimental and Density Functional Theory Simulation Studies. *ACS Appl. Mater. Interfaces* **2019**, *11*, 10697–10706.
- (23) Battu, A. K.; Zade, V. B.; Deemer, E.; Ramana, C. V. Microstructure-Mechanical Property Correlation in Size Controlled Nanocrystalline Molybdenum Films. *Adv. Eng. Mater.* **2018**, *20*, 1800496.
- (24) Hussain, O. M.; Srinivasa Rao, K.; Madhuri, K. V.; Ramana, C. V.; Naidu, B. S.; Pai, S.; John, J.; Pinto, R. Growth and characteristics of reactive pulsed laser deposited molybdenum trioxide thin films. *Appl. Phys. A Mater. Sci. Process* **2002**, *75*, 417–422.
- (25) Kibsgaard, J.; Tsai, C.; Chan, K.; Benck, J. D.; Nørskov, J. K.; Abild-Pedersen, F.; Jaramillo, T. F. Designing an improved transition metal phosphide catalyst for hydrogen evolution using experimental and theoretical trends. *Energy Environ. Sci.* **2015**, *8*, 3022–3029.
- (26) Kibsgaard, J.; Jaramillo, T. F. Molybdenum Phosphosulfide: An Active, Acid-Stable, Earth-Abundant Catalyst for the Hydrogen Evolution Reaction. *Angew. Chem., Int. Ed* **2014**, *53*, 14433–14437.
- (27) Nikam, R. D.; Lu, A.-Y.; Sonawane, P. A.; Kumar, U. R.; Yadav, K.; Li, L.-J.; Chen, Y.-T. Three-Dimensional Heterostructures of MoS<sub>2</sub> Nanosheets on Conducting MoO<sub>2</sub> as an Efficient Electrocatalyst To Enhance Hydrogen Evolution Reaction. *ACS Appl. Mater. Interfaces* **2015**, *7*, 23328–23335.
- (28) Wang, F.; He, P.; Li, Y.; Shifa, T. A.; Deng, Y.; Liu, K.; Wang, Q.; Wang, F.; Wen, Y.; Wang, Z.; Zhan, X.; Sun, L.; He, J. Interface Engineered  $W_x C@WS_2$  Nanostructure for Enhanced Hydrogen Evolution Catalysis. *Adv. Funct. Mater.* **2017**, *27*, 1605802.
- (29) Zhou, X.; Liu, Y.; Ju, H.; Pan, B.; Zhu, J.; Ding, T.; Wang, C.; Yang, Q. Design and Epitaxial Growth of MoSe<sub>2</sub>–NiSe Vertical Heteronanostructures with Electronic Modulation for Enhanced Hydrogen Evolution Reaction. *Chem. Mater.* **2016**, *28*, 1838–1846.
- (30) Yang, L.; Zhou, W.; Hou, D.; Zhou, K.; Li, G.; Tang, Z.; Li, L.; Chen, S. Porous metallic MoO<sub>2</sub>-supported MoS<sub>2</sub> nanosheets for enhanced electrocatalytic activity in the hydrogen evolution reaction. *Nanoscale* **2015**, *7*, 5203–5208.
- (31) Yang, Y.; An, X.; Kang, M.; Guo, F.; Zhang, L.; Wang, Q.; Sun, D.; Liao, Y.; Yang, Z.; Lei, Z. Distinctive  $MoS_2$ -MoP nanosheet structures anchored on N-doped porous carbon support as a catalyst to enhance the electrochemical hydrogen production. *New. J. Chem.* **2021**, *45*, 14042–14049.
- (32) Loomba, S.; Khan, M. W.; Haris, M.; Mousavi, S. M.; Zavabeti, A.; Xu, K.; Tadich, A.; Thomsen, L.; McConville, C. F.; Li, Y.; Walia, S.; Mahmood, N. Nitrogen-Doped Porous Nickel Molybdenum Phosphide Sheets for Efficient Seawater Splitting. *Small* **2023**, *19*, 2207310.
- (33) Gu, Y.; Wu, A.; Jiao, Y.; Zheng, H.; Wang, X.; Xie, Y.; Wang, L.; Tian, C.; Fu, H. Two-Dimensional Porous Molybdenum Phosphide/Nitride Heterojunction Nanosheets for pH-Universal Hydrogen Evolution Reaction. *Angew. Chem., Int. Ed.* **2021**, *60*, 6673–6681.

- (34) Calvillo, L.; Carraro, F.; Vozniuk, O.; Celorrio, V.; Nodari, L.; Russell, A. E.; Debellis, D.; Fermin, D.; Cavani, F.; Agnoli, S.; Granozzi, G. Insights into the durability of Co–Fe spinel oxygen evolution electrocatalysts via operando studies of the catalyst structure. *J. Mater. Chem. A* **2018**, *6*, 7034–7041.
- (35) Zhu, Y.; Wang, J.; Chu, H.; Chu, Y.-C.; Chen, H. M. In Situ/Operando Studies for Designing Next-Generation Electrocatalysts. *Acs. Energy. Lett.* **2020**, *5*, 1281–1291.
- (36) Liu, Y.; Wu, J.; Hackenberg, K. P.; Zhang, J.; Wang, Y. M.; Yang, Y.; Keyshar, K.; Gu, J.; Ogitsu, T.; Vajtai, R.; Lou, J.; Ajayan, P. M.; Wood, B. C.; Yakobson, B. I. Self-optimizing, highly surface-active layered metal dichalcogenide catalysts for hydrogen evolution. *Nat. Energy* **2017**, *2*, 17127.
- (37) Nam, D.-H.; Bushuyev, O. S.; Li, J.; De Luna, P.; Seifitokaldani, A.; Dinh, C.-T.; Wang, Y.; Liang, Z.; Proppe, A. H.; Tan, C. S.; Todorović, P.; Shekhah, O.; Gabardo, C. M.; Jo, J. W.; Choi, J.; Choi, M.-J.; Baek, S.-W.; Kim, J.; Sinton, D.; Kelley, S. O.; Eddaoudi, M.; Sargent, E. H. Metal—Organic Frameworks Mediate Cu Coordination for Selective CO<sub>2</sub> Electroreduction. *J. Am. Chem. Soc.* **2018**, *140*, 11378—11386.
- (38) Ji, P.; Luo, X.; Chen, D.; Jin, H.; Pu, Z.; Zeng, W.; He, J.; Bai, H.; Liao, Y.; Mu, S. Significantly Improved Water Oxidation of CoP Catalysts by Electrochemical Activation. *ACS Sustain. Chem. Eng.* **2020**, *8*, 17851–17859.
- (39) Su, L.; Cui, X.; He, T.; Zeng, L.; Tian, H.; Song, Y.; Qi, K.; Xia, B. Y. Surface reconstruction of cobalt phosphide nanosheets by electrochemical activation for enhanced hydrogen evolution in alkaline solution. *Chem. Sci.* **2019**, *10*, 2019–2024.
- (40) Jiang, H.; He, Q.; Zhang, Y.; Song, L. Structural Self-Reconstruction of Catalysts in Electrocatalysis. *Acc. Chem. Res.* **2018**, *51*, 2968–2977.
- (41) Das, D.; Gutierrez, G.; Ramana, C. V. Raman Spectroscopic Characterization of Chemical Bonding and Phase Segregation in Tin (Sn)-Incorporated  $Ga_2O_3$ . ACS Omega 2023, 8, 11709–11716.
- (42) Roy, S.; Ramana, C. V. Effect of sintering temperature on the chemical bonding, electronic structure and electrical transport properties of  $\beta$ -Ga<sub>1.9</sub>Fe<sub>0.1</sub>O<sub>3</sub> compounds. *J. Mater. Sci. Technol.* **2021**, *67*, 135–144.
- (43) Fairley, N.; Carrick, A.; Fairly, N. *The casa cookbook*; Acolyte science Cheshire, 2005; Vol. 1.
- (44) Ramana, C. V.; Roy, S.; Zade, V.; Battu, A. K.; Makeswaran, N.; Shutthanandan, V. Electronic structure and chemical bonding in transition-metal-mixed gallium oxide (Ga<sub>2</sub>O<sub>3</sub>) compounds. *J. Phys. Chem. Solids* **2021**, *157*, 110174.
- (45) Ramana, C. V.; Bandi, M.; N Nair, A.; Manciu, F. S.; Sreenivasan, S.; Shutthanandan, V. Electronic Structure, Chemical Bonding, and Electrocatalytic Activity of Ba(Fe<sub>0.7</sub>Ta<sub>0.3</sub>)O<sub>3-δ</sub> Compounds. *ACS Appl. Energy Mater* **2021**, *4*, 1313–1322.
- (46) Pinaeva, L.; Prosvirin, I.; Chesalov, Y.; Atuchin, V. High-Temperature Abatement of  $N_2O$  over  $FeO_x/CeO_2$ - $Al_2O_3$  Catalysts: The Effects of Oxygen Mobility Catalysts. *Catalysts.* **2022**, 938. DOI:.
- (47) Nadeina, K. A.; Budukva, S. V.; Vatutina, Y. V.; Mukhacheva, P. P.; Gerasimov, E. Y.; Pakharukova, V. P.; Prosvirin, I. P.; Larina, T. V.; Klimov, O. V.; Noskov, A. S.; Atuchin, V. V. Optimal Choice of the Preparation Procedure and Precursor Composition for a Bulk Ni–Mo–W Catalyst. *Inorganics* **2023**, *11*, 89.
- (48) Valle, E.; Duyar, M. S.; Snider, J. L.; Regli, S. K.; Rønning, M.; Gallo, A.; Jaramillo, T. F. In Situ Studies of the Formation of MoP Catalysts and Their Structure under Reaction Conditions for Higher Alcohol Synthesis: The Role of Promoters and Mesoporous Supports. *J. Phys. Chem. C* **2022**, *126*, 5575–5583.
- (49) Wei, Z. B. Z.; Grange, P.; Delmon, B. XPS and XRD studies of fresh and sulfided Mo<sub>2</sub>N. Appl. Surf. Sci. 1998, 135, 107–114.
- (50) Bull, C. L.; Kawashima, T.; McMillan, P. F.; Machon, D.; Shebanova, O.; Daisenberger, D.; Soignard, E.; Takayama-Muromachi, E.; Chapon, L. C. Crystal structure and high-pressure properties of  $\gamma$ -Mo<sub>2</sub>N determined by neutron powder diffraction and X-ray diffraction. *J. Solid State Chem.* **2006**, *179*, 1762–1767.

- (51) Guevara, A.; Alvarez, A.; Vrinat, M. Effect of TiO<sub>2</sub>–Al<sub>2</sub>O<sub>3</sub> Sol–Gel Supports on the Superficial Ni and Mo Species in Oxidized and Sulfided NiMo/TiO<sub>2</sub>–Al<sub>2</sub>O<sub>3</sub> Catalysts: Influence on Dibenzothiophene Hydrodesulfurization. *Catal. Lett.* **2008**, *126*, 268–274.
- (52) Gong, L.; Haur, S. C. On demand rapid patterning of colored amorphous molybdenum oxide using a focused laser beam. *J. Mater. Chem. C* **2017**, *5*, 2090–2097.
- (53) Camacho-Lopez, S.; Cano-Lara, M.; Camacho-Lopez, M. Fast Growth of Multi-Phase MoO<sub>x</sub> Synthesized by Laser Direct Writing Using Femtosecond Pulses. *Crystals* **2020**, *10*, 629.
- (54) Deng, C.; Ding, F.; Li, X.; Guo, Y.; Ni, W.; Yan, H.; Sun, K.; Yan, Y.-M. Templated-preparation of a three-dimensional molybdenum phosphide sponge as a high performance electrode for hydrogen evolution. *J. Mater. Chem. A* **2016**, *4*, 59–66.
- (55) Baraskar, B. G.; Kolekar, Y. D.; Thombare, B. R.; James, A. R.; Kambale, R. C.; Ramana, C. V. Enhanced Piezoelectric, Ferroelectric, and Electrostrictive Properties of Lead-Free (1-x)BCZT-(x)BCST Electroceramics with Energy Harvesting Capability. *Small* **2023**, *19*, 2300549.
- (56) Ramana, C. V.; Ait-Salah, A.; Utsunomiya, S.; Mauger, A.; Gendron, F.; Julien, C. M. Novel Lithium Iron Pyrophosphate (LiFe<sub>1.5</sub>P<sub>2</sub>O<sub>7</sub>) as a Positive Electrode for Li-Ion Batteries. *Chem. Mater.* **2007**, *19*, 5319–5324.
- (57) Ramana, C. V.; Bharathi, K. K.; Garcia, A.; Campbell, A. L. Growth Behavior, Lattice Expansion, Strain, and Surface Morphology of Nanocrystalline, Monoclinic HfO<sub>2</sub> Thin Films. *J. Phys. Chem. C* **2012**, *116*, 9955–9960.
- (58) Makeswaran, N.; Das, D.; Zade, V.; Gaurav, P.; Shutthanandan, V.; Tan, S.; Ramana, C. V. Size- and Phase-Controlled Nanometer-Thick  $\beta$ -Ga<sub>2</sub>O<sub>3</sub> Films with Green Photoluminescence for Optoelectronic Applications. *Acs Appl. Nano Mater.* **2021**, *4*, 3331–3338.
- (59) Nalam, P. G.; Das, D.; Tan, S.; Ramana, C. V. Controlled Phase Stabilization Enabled Tunable Optical Properties of Nanocrystalline GeO<sub>2</sub> Films. *ACS Appl. Electron. Mater* **2022**, *4*, 3115–3124.
- (60) Zhang, S.; Yao, Y.; Jiao, X.; Ma, M.; Huang, H.; Zhou, X.; Wang, L.; Bai, J.; Yu, Y. Mo<sub>2</sub>N–W<sub>2</sub>N Heterostructures Embedded in Spherical Carbon Superstructure as Highly Efficient Polysulfide Electrocatalysts for Stable Room-Temperature Na–S Batteries. *Adv. Mater.* **2021**, 33, 2103846.
- (61) Gruenert, W.; Stakheev, A. Y.; Feldhaus, R.; Anders, K.; Shpiro, E. S.; Minachev, K. M. Analysis of molybdenum(3d) XPS spectra of supported molybdenum catalysts: an alternative approach. *J. Phys. Chem.* 1991, 95, 1323–1328.
- (62) Liu, Q.; Xue, Z.; Jia, B.; Liu, Q.; Liu, K.; Lin, Y.; Liu, M.; Li, Y.; Li, G. Hierarchical Nanorods of MoS<sub>2</sub>/MoP Heterojunction for Efficient Electrocatalytic Hydrogen Evolution Reaction. *Small* **2020**, *16*, 2002482.
- (63) Pandey, S. A.; Zhang, C.; Ibrahim, D. H.; Goldfine, E. A.; Wenderott, J. K.; dos Reis, R.; Paul, R. L.; Spanopoulos, I.; Kanatzidis, M.; Bedzyk, M. J.; Dravid, V. P.; González, G. B.; Haile, S. M. Hidden Complexity in the Chemistry of Ammonolysis-Derived "γ-Mo<sub>2</sub>N": An Overlooked Oxynitride Hydride. *Chem. Mater.* **2021**, 33, 6671–6684. (64) Saleh, A. A.; Sayed, D. M.; Nagle-Cocco, L. A. V.; Divitini, G.;
- Ghanem, L. G.; Ducati, C.; Allam, N. K. Deciphering the In Situ Surface Reconstruction of Supercapacitive Bimetallic Ni-Co Oxyphosphide during Electrochemical Activation Using Multivariate Statistical Analyses. ACS Appl. Energy Mater. 2022, 5, 7661–7673.
- (65) Liu, J.; Tang, S.; Lu, Y.; Cai, G.; Liang, S.; Wang, W.; Chen, X. Synthesis of  $Mo_2N$  nanolayer coated  $MoO_2$  hollow nanostructures as high-performance anode materials for lithium-ion batteries. *Energy Environ. Sci.* **2013**, *6*, 2691–2697.
- (66) Jiao, Y.-Q.; Yan, H.-J.; Tian, C.-G.; Fu, H.-G. Structure Engineering and Electronic Modulation of Transition Metal Interstitial Compounds for Electrocatalytic Water Splitting. *Acc. Mater. Res.* **2023**, *4*, 42–56.
- (67) Liu, S.; Hu, C.; Lv, C.; Cai, J.; Duan, M.; Luo, J.; Song, J.; Shi, Y.; Chen, C.; Luo, D.; Watanabe, A.; Aoyagi, E.; Ito, S. Facile preparation of large-area self-supported porous nickel phosphide

nanosheets for efficient electrocatalytic hydrogen evolution. *Int. J. Hydrog. Energy* **2019**, *44*, 17974–17984. (68) Murthy, A. P.; Theerthagiri, J.; Madhavan, J. Insights on Tafel Constant in the Analysis of Hydrogen Evolution Reaction. *J. Phys. Chem. C* **2018**, *122*, 23943–23949.